UCLA
UCLA Previously Published Works

Title
Artificial Photosynthesis on TiO2-Passivated InP Nanopillars

Permalink
https://escholarship.org/uc/item/4jp915pd

Journal
Nano Letters, 15(9)

ISSN
1530-6984

Authors
Qiu, Jing
Zeng, Guangtong
Ha, Mai-Anh
et al.

Publication Date
2015-09-09

DOI
10.1021/acs.nanolett.5b02511

Peer reviewed

eScholarship.org Powered by the California Digital Library
University of California

NANO LETTERS

Letter

pubs.acs.org/NanoLett

Artificial Photosynthesis on TiO_2-Passivated InP Nanopillars

Jing Qiu,[‡] Guangtong Zeng,[†] Mai-Anh Ha,[∥] Mingyuan Ge,[†] Yongjing Lin,[⊥] Mark Hettick,[⊥] Bingya Hou,[§] Anastassia N. Alexandrova,[∥,⊥] Ali Javey,[#] and Stephen B. Cronin*[,†,§]

[†]Department of Chemistry, [‡]Department of Materials Science, and [§]Department of Electrical Engineering, University of Southern California, Los Angeles, California 90089, United States

[∥]Department of Chemistry and Biochemistry, [⊥]California NanoSystems Institute, University of California Los Angeles, Los Angeles, California 90025, United States

[#]Material Sciences Division, Lawrence Berkeley National Laboratory, Berkeley, California 94720, United States

Supporting Information

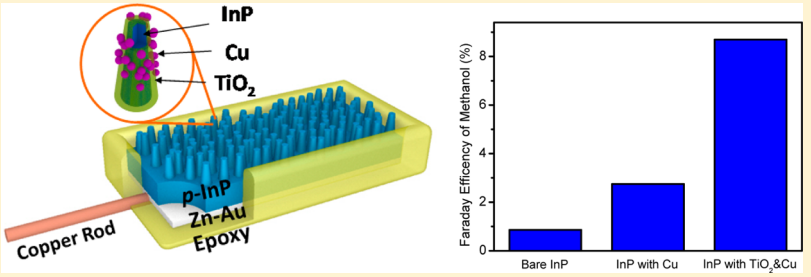

ABSTRACT: Here, we report photocatalytic CO_2 reduction with water to produce methanol using TiO_2-passivated InP nanopillar photocathodes under 532 nm wavelength illumination. In addition to providing a stable photocatalytic surface, the TiO_2-passivation layer provides substantial enhancement in the photoconversion efficiency through the introduction of O vacancies associated with the nonstoichiometric growth of TiO_2 by atomic layer deposition. Plane wave-density functional theory (PW-DFT) calculations confirm the role of oxygen vacancies in the TiO_2 surface, which serve as catalytically active sites in the CO_2 reduction process. PW-DFT shows that CO_2 binds stably to these oxygen vacancies and CO_2 gains an electron (−0.897e) spontaneously from the TiO_2 support. This calculation indicates that the O vacancies provide active sites for CO_2 absorption, and no overpotential is required to form the CO_2^- intermediate. The TiO_2 film increases the Faraday efficiency of methanol production by 5.7× to 4.79% under an applied potential of −0.6 V vs NHE, which is 1.3 V below the $E^o(CO_2/CO_2^-) = -1.9$ eV standard redox potential. Copper nanoparticles deposited on the TiO_2 act as a cocatalyst and further improve the selectivity and yield of methanol production by up to 8-fold with a Faraday efficiency of 8.7%.

KEYWORDS: *Photoelectrochemical, InP, copper, CO_2 reduction, TiO_2-passivation, methanol*

Downloaded by UNIV OF CALIFORNIA LOS ANGELES on September 1, 2015 | http://pubs.acs.org
Publication Date (Web): August 14, 2015 | doi: 10.1021/acs.nanolett.5b02511

With the rising level of CO_2 in the earth's atmosphere, artificial photosynthesis (i.e., a process that utilizes sunlight to convert water and carbon dioxide into carbohydrates) has begun to receive increasing attention by researchers around the world. In 1978, Halmann et al. reported the first photocatalytic reduction of CO_2 to hydrocarbons, including formic acid, formaldehyde, and methanol. This pioneering work utilized *p*-type GaP under 365 nm wavelength illumination with an applied overpotential of −1.4 V (vs SCE).[1] Many attempts have since been made to reduce CO_2 to hydrocarbons under UV illumination.[2−4] However, few researchers have achieved photoreduction under visible illumination due to the limited selection of materials.[5] For optimum solar utilization, the band gap of the semiconductor should lie in the range of 1.2−1.4 eV, as derived in the Schokley−Quiesser limit.[6] Also, the position of the conduction band (i.e., electron affinity) must be as close as possible to the CO_2 to CO_2^- redox potential (−1.9 V vs NHE) in order to minimize the applied overpotential required to drive this reaction.[7] Since the energy needed to reach the CO_2^- intermediate is so high, a cocatalyst is usually added to lower the energy barrier of this intermediate species. Lastly, the surface recombination rate of the photon-induced electron hole pairs should be as low as possible. InP is a promising material for CO_2 reduction since its band gap of 1.34 eV is well-matched to the solar spectrum. Furthermore, the surface-recombination velocity of untreated InP is low (ca. 10^4 cm/s for n-type and 10^5 cm/s for p-type).[7] Nanotexturing of InP can further enhance the photon-to-chemical energy conversion efficiency due to the increase in surface area and reduced reflection.[8] CO_2 reduction to methanol on p-InP has been reported at relatively high applied potentials of −1.3 V (vs SCE) and with low Faraday efficiencies (around 1%).[3] Both the poor selectivity for methanol production with respect to H_2 and severe photo-

Received: June 24, 2015
Revised: July 30, 2015

 © XXXX American Chemical Society

DOI: 10.1021/acs.nanolett.5b02511
Nano Lett. XXXX, XXX, XXX−XXX

corrosion have limited the application of InP in the artificial photosynthesis of hydrocarbons.

Here, we utilize TiO_2-passivated nanotextured InP photocathodes to explore aqueous CO_2 reduction to methanol under 532 nm illumination as a function of applied potential. The selectivity of methanol production is compared for InP samples prepared with and without Cu nanoparticles and TiO_2-passivation layers. The photocatalytic surface is characterized by high resolution transmission electron microscopy (HRTEM) in order to provide a detailed picture of the nanoparticle/TiO_2/InP interface. Plane wave density functional theory (PW-DFT) calculations are carried out to explore the role of surface binding of reactants and intermediate species to the TiO_2 surface.

A schematic diagram of the sample geometry is illustrated in Figure 1a. Zn-doped *p*-type (100) oriented InP nanopillars

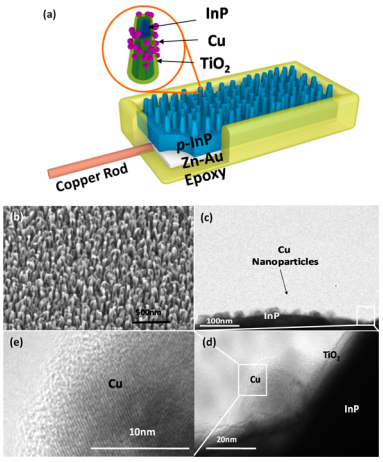

Figure 1. (a) Schematic diagram of TiO_2-passivated InP nanopillars with Cu cocatalyst nanoparticles. (b–e) SEM and TEM images of InP nanopillar array with TiO_2 deposition layer and Cu nanoparticles. The high resolution TEM image in (e) resolves the crystal lattice of the Cu nanoparticles.

(NPLs) with a dopant concentration of 5×10^{17} cm^{-3} were used as the photocatalyst for CO_2 reduction. The InP NPLs are around 80 nm in diameter and approximately 400 to 600 nm tall and have an average pitch of approximately 50 nm (Figure 1b). A detailed description of the InP NPLs preparation is provided in the Supporting Information. Briefly, InP bulk wafers are treated in a reactive ion O_2 plasma treatment followed by a 2 min wet-etching step in HCl/H_3PO_4 (3:1) to remove the surface-damaged layers and contaminants.[8] Atomic layer deposition (ALD) of TiO_2 was performed at 250 °C on the *p*-InP wafers with $TiCl_4$ as the titanium source and water vapor as the oxygen source. The average rate of deposition is approximately 0.44 Å per cycle, as calibrated by ellipsometry. We then evaporate copper with a nominal thickness of 0.5 nm on the top surface of the TiO_2. A Zn–Au film was evaporated on the back of the *p*-InP to form an Ohmic contact. The Zn–Au contact was then connected to the external circuitry with a copper wire and coated with epoxy cement to insulate it from the electrolytic solution. A schematic diagram of the sample geometry is illustrated in Figure 1a. Figure 1c–e shows transmission electron microscope (TEM) images of the 0.5 nm Cu on the top of the InP NPLs. These figures indicate that, instead of forming a uniform continuous film, the evaporated 0.5 nm Cu forms crystal nanoparticles with diameters around 20 nm. In Figure 1e, a thin amorphous layer of CuO can be seen on the surface of the Cu nanoparticles, which is formed in air. The XPS spectra shown in Figure S8 of the Supporting Information confirms the existence of Cu 2p and O 1s peaks corresponding to CuO. The thickness of the deposited TiO_2 is around 3 nm, as shown in Figure 1d. A three-terminal potentiostat was used with the prepared semiconductor samples as the working electrode, a Ag/AgCl electrode as the reference electrode, and a Pt electrode functioning as the counter electrode. The photocatalytic reaction rates of two sets of samples were measured in a 0.5 M KCl solution, while continuously bubbling CO_2 through the solution. The products are detected using NMR spectroscopy and gas chromatography (GC). A schematic diagram of the photoelectrochemical measurement setup is shown in Figure S6 of the Supporting Information.

While photocatalytic CO_2 reduction on InP and other III–V compound semiconductors has been demonstrated previously,[3,5] these materials corrode rapidly under photoelectrochemical conditions and are significantly degraded after just 30 min of illumination.[9,10] Several research groups have shown that by depositing thin films of TiO_2 on these unstable semiconductors, they can be protected from corrosion.[8−12] In order to make InP photochemically stable, we passivated the surface using a 3 nm thin film of TiO_2 deposited by ALD, as illustrated schematically in Figure 1a. Under 532 nm illumination, the photocurrent of InP nanopillars with TiO_2-passivation is stable for at least 12 h, as shown in Figure S1 in the Supporting Information.

Figure 2a shows the photocurrent–voltage curves measured in a 0.5 M KCl solution under 532 nm illumination for bare InP nanopillars and InP nanopillars passivated with TiO_2. With TiO_2-passivation, the photocurrent is substantially increased for all applied potentials. The bare InP nanopillar sample (blue curve) has an onset of photocurrent at a potential of approximately 0.03 V (vs NHE), as indicated in Figure 2b. For TiO_2-passivated InP (red curve), we observe a clear shift in the onset potential by about 0.1 V in these photo-*I*–*V* characteristics. We attribute this, in part, to a *pn*-junction formed between the TiO_2, which is *n*-type due to oxygen vacancies, and the *p*-type InP.[9,13] This *pn*-junction creates a built-in potential that assists in the separation of photogenerated electron–hole pairs and results in a shift of the onset potential of this reaction. Figure 2c shows the methanol peaks observed in the NMR spectra of bare InP nanopillars and TiO_2-passivated InP nanopillars after 12 h reactions at an applied potential of −0.6 V vs NHE under 532 nm illumination, as shown in the energy band diagram of this photocatalytic system (Figure S7 of the Supporting Information). If we consider the one electron reduction of CO_2 to CO_2^- as the first step on this reaction, this is 1.3 V below the $E^o(CO_2/CO_2^-) = -1.9$ eV standard redox potential. Figure 2d shows the Faraday efficiencies of methanol (i.e., the selectivity of methanol) for these two types of samples. This figure indicates that the TiO_2-passivation layer not only enhances the overall photon-conversion efficiency but also increases the selectivity of methanol from H_2 and other hydrocarbons from 0.85% to 4.8%. We attribute the increased methanol selectivity to oxygen vacancies that are inherent to these thin TiO_2 films, which provide the catalytically active sites for CO_2 reduction.[14−16] Peaks corresponding to Ti^{3+} states (i.e., O-vacancies) are observed in the XPS spectra taken from TiO_2 deposited on InP, as shown in Figure S5 of the Supporting Information.

Downloaded by UNIV OF CALIFORNIA LOS ANGELES on September 1, 2015 | http://pubs.acs.org
Publication Date (Web): August 14, 2015 | doi: 10.1021/acs.nanolett.5b02511

DOI: 10.1021/acs.nanolett.5b02511
Nano Lett. XXXX, XXX, XXX–XXX

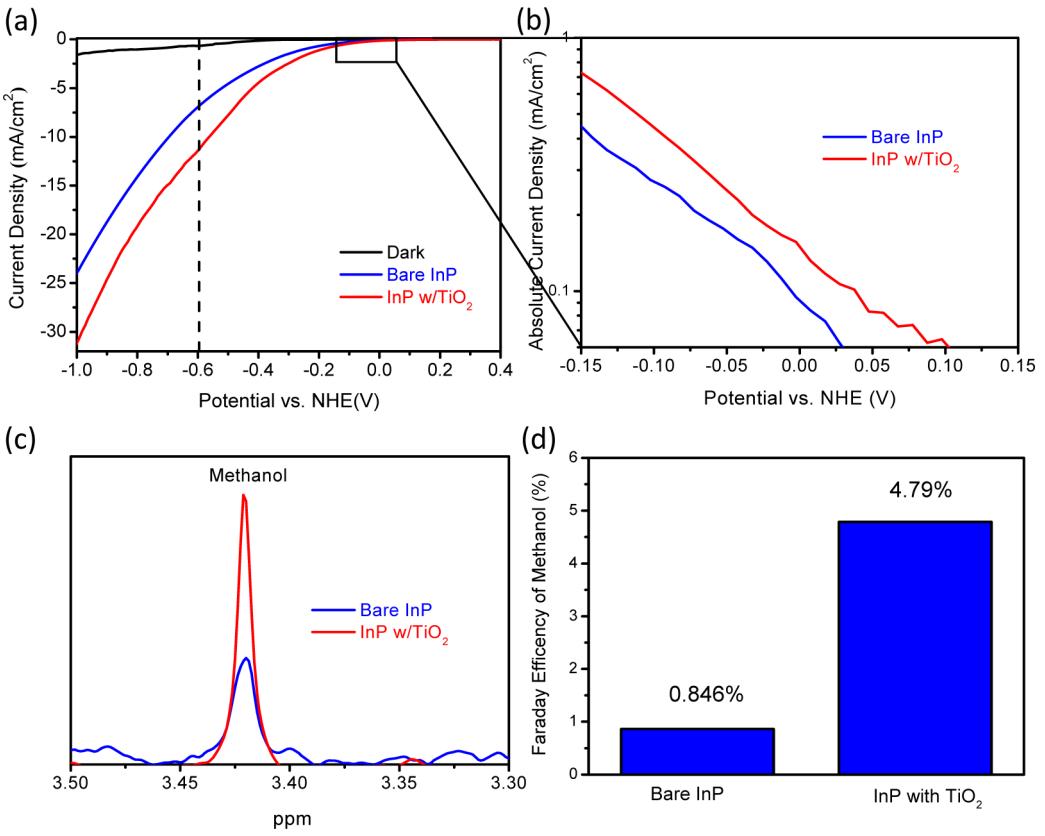

Figure 2. (a) Photocatalytic current−potential curves where the dashed line indicates the potential applied during the methanol test. (b) Log plot of photocatalytic current−potential curves. (c) Methanol peak in NMR spectra and (d) Faraday efficiencies of methanol production for InP nanopillars with and without 3 nm TiO_2 under 532 nm illumination in a CO_2 saturated 0.5 M KCl solution.

In order to verify the role of these oxygen vacancies in the photocatalytic reduction of CO_2, all plane wave density functional theory (PW-DFT) calculations were performed with the Quantum Espresso package using the most recently available ultrasoft pseudopotentials with scalar relativistic corrections,[17−20] and spin-unrestricted calculations were done employing the Perdew−Burke−Ernzerhof (PBE) functional.[21] Clean, stoichiometric anatase and defective anatase with an oxygen vacancy were both investigated in this study. Details of the calculation are given in the Supporting Information. The DFT+U approach was adopted in order to recover these highly localized states with a self-consistently computed U term of 3.6 eV applied to Ti atoms, well within Finazzi et al.'s suggested range of 3−4 eV for anatase.[22,23] Although one study found the oxygen vacancy to be present deep in slabs of varying size,[24] others were unable to determine the most stable vacancy structure.[13] Our DFT+U calculations identified the oxygen vacancy to be at the surface, specifically, the 2-fold coordinated bridging oxygen (see Figure 3), as energetically favorable compared to other sites. Adsorption energies were calculated by subtracting the two components (molecule and surface) from the adsorbed system:

$$E_{ads} = E[\text{surf} + \text{molecule}] - E[\text{surf}] - E[\text{molecule}]$$

where the molecule was H_2O, CO_2, or CO_2^- and the surface, stoichiometric anatase or defective anatase with a surface oxygen vacancy. A thorough, manual search was performed to determine the global minimum of adsorbed molecules to the anatase support. Adsorption energies were favorable between neutral CO_2 adsorbed to stoichiometric (−0.48 eV) and

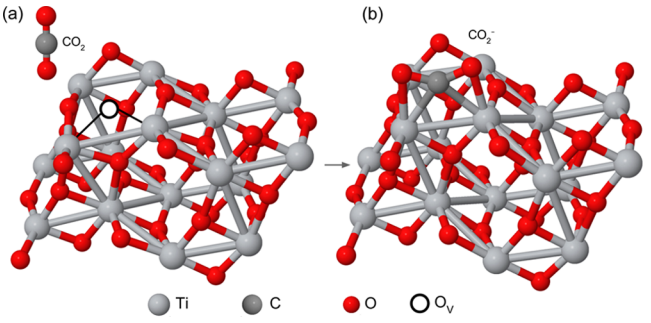

Figure 3. PW-DFT calculated structure for anatase TiO_2 with O vacancies (a) before CO_2 adsorption and (b) after CO_2 adsorption and relaxation.

defective anatase (−0.94 eV), as illustrated in Figure 3. The global minima found reproduced the geometries of Sorescu et al.'s PW-DFT study of the adsorption of CO_2 on anatase.[34] The difference in adsorption energies to Sorescu et al.'s results may be attributed to our smaller cell and computational parameter (see Supporting Information for details). In our study, we investigated alternative roles of the anatase support such as stabilization of CO^{2-} intermediate. However, the adsorption of CO_2^- to stoichiometric and defective anatase resulted in repulsive, unstable systems, requiring thermodynamically unfavorable energies of 4.39 and 2.57 eV, respectively, to form. The chemical bonding analysis obtained using the Bader charge localization scheme is shown in Figure S3 in the Supporting Information.[25−27] In Figure 2b, the linear CO_2 molecule becomes bent upon adsorption to the defective

Downloaded by UNIV OF CALIFORNIA LOS ANGELES on September 1, 2015 | http://pubs.acs.org
Publication Date (Web): August 14, 2015 | doi: 10.1021/acs.nanolett.5b02511

DOI: 10.1021/acs.nanolett.5b02511
Nano Lett. XXXX, XXX, XXX−XXX

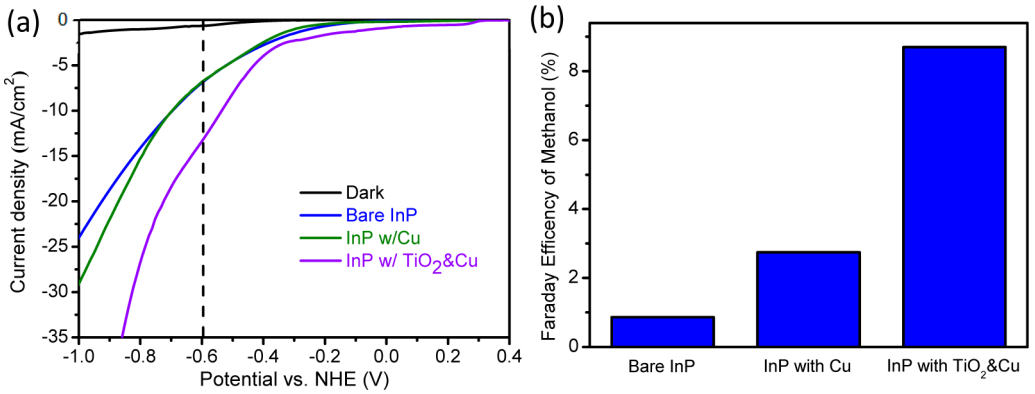

Figure 4. (a) Photocatalytic current−potential curves and (b) Faraday efficiencies of methanol production for samples of bare InP, InP/Cu, and InP/TiO_2/Cu under 532 nm illumination in a CO_2 saturated 0.5 M KCl solution for a 12 h reaction.

Downloaded by UNIV OF CALIFORNIA LOS ANGELES on September 1, 2015 | http://pubs.acs.org
Publication Date (Web): August 14, 2015 | doi: 10.1021/acs.nanolett.5b02511

anatase support, its C effectively filling the bridging oxygen vacancy. Moreover, CO_2 gains an electron (−0.897e) spontaneously from the TiO_2 support. This calculation indicates that the O vacancies provide active sites for CO_2 absorption, and no overpotential is required to form the CO_2^- intermediate. In fact, 4 of the 8 minima found by Sorescu et al. formed the CO^{2-} intermediate.[34] These CO_2^- intermediates then react with H_2O to form methanol. Therefore, this thin TiO_2 film can not only protect InP from photocorrosion, but also increase the methanol yields without applying high overpotentials.

In order to further improve the selectivity of methanol with respect to H_2 evolution in aqueous solution, we deposited copper nanoparticles on the TiO_2-passivated InP nanopillars. Cu and its oxide are known catalysts for CO_2 reduction by lowering the energy barriers of intermediate states in the reaction[28,29] and have been intensively studied in the electrochemical reduction of CO_2.[30,31] Figure 4a shows the photo-*I*−*V* characteristics of InP nanopillars with copper nanoparticles (green curve) and TiO_2-passivated InP nanopillars with copper (purple line). From this Figure, we find that the addition of Cu nanoparticles to the bare InP NPLs (green curve) does not change the photo-*I*−*V* characteristics. However, it does increase the Faraday efficiency of methanol from 0.85% to 2.8%, indicating that copper is an active catalyst for CO_2 reduction to methanol. By deposition of copper nanoparticles on the TiO_2-passivated InP nanopillars, we successfully increase the selectivity to 8.7%, as shown in Figure 4b. This improvement in the selectivity likely results from the interface of the copper nanoparticles and the TiO_2-passivation layer. For Cu as a metal catalyst (and likely CuO), there have been several previous works reporting that it has a moderate hydrogen overvoltage and weak CO_2 adsorption characteristics, and that it can facilitate the reaction of CO with H_2 to generate hydrocarbons, aldehydes, and alcohols as major products.[30,32] We believe it is the oxygen vacancies in the TiO_2 and Cu together that promote the selectivity of methanol over H_2 production; however, a detailed reaction mechanism is still under investigation.

The previous work of Lee et al. showed that these nanotextured InP photocathodes exhibit about a 40% enhancement in the photoconversion efficiency compared to planar surfaces in photocatalytic water splitting.[8] In the work presented here, we also observed an enhancement by a factor of 2 in total conversion efficiency when comparing InP nanopillars to planar InP. The Faraday efficiencies of methanol production, however, are around 1% for both planar and nanopillar InP, and thus, the selectivity of methanol with respect to H_2 is almost the same, as listed in Table S1 in the Supporting Information. By depositing Cu nanoparticles on TiO_2-passivated InP nanopillars, the Faraday efficiency increases to 8.7%. The H_2 yields produced by these samples were measured by GC after 12 h of illumination with 532 nm wavelength light under an applied potential of −0.6 V vs NHE, as shown in Figure 5. Table 1 lists the H_2 yields from these GC

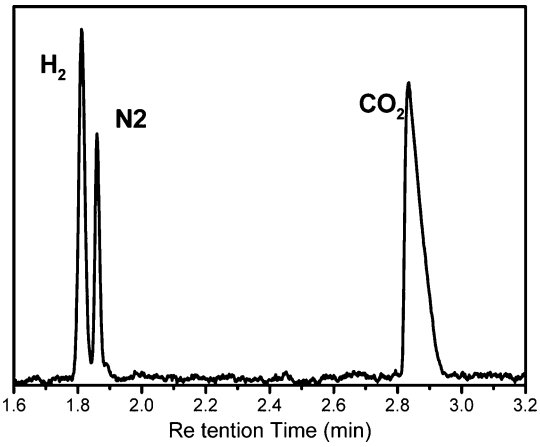

Figure 5. Gas chromatograph (GC) data taken after 12 h reaction on InP/TiO_2/Cu sample under 532 nm illumination in a CO_2 saturated 0.5 M KCl solution.

Table 1. Faraday Efficiencies of Hydrogen and Methanol of 12 h Reaction on InP/TiO_2/Cu Sample under 532 nm Illumination in a CO_2 Saturated 0.5M KCl Solution

3 nm TiO_2 and Cu	H_2	CH_3OH	H_2 and CH_3OH
Faraday efficiency	76.9%	8.7%	85.6%

measurements, methanol yields from NMR spectroscopy, and the total integrated charge running through the device. For 3 nm TiO_2-passivated InP nanopillars, the Faraday efficiency is 83.6% in total and 76.9% for H_2 evolution. This indicates that, in aqueous solution, simultaneous H_2 evolution is an inevitable competing reaction with a lower energy barrier than CO_2 reduction. In order to suppress the H_2 competing reaction, a nonaqueous solution should be used in future studies.

In summary, photocatalytic CO_2 reduction with water to produce methanol is observed using TiO_2-passivated InP

DOI: 10.1021/acs.nanolett.5b02511
Nano Lett. XXXX, XXX, XXX−XXX

nanopillar photocathodes under 532 nm wavelength illumination. In addition to providing a stable photocatalytic surface, the TiO_2-passivation provides substantial enhancement in the photoconversion efficiency through the introduction of O vacancies associated with the nonstoichiometric growth of TiO_2 by atomic layer deposition. The role of these oxygen vacancies as catalytically active sites in the photocatalytic reduction of CO_2 is established by PW-DFT calculations, which indicate that CO_2 binds stably to these oxygen vacancies and gains an electron (−0.897e) spontaneously from the TiO_2 support. Therefore, no externally applied overpotential is required to form the CO_2^- intermediate, which can subsequently react with H_2O to form methanol. Copper nanoparticles deposited on the TiO_2 act as a cocatalyst, which further improves the selectivity and yield of methanol production by up to 8-fold giving a Faraday efficiency of 8.7%.

■ ASSOCIATED CONTENT

Supporting Information

The Supporting Information is available free of charge on the ACS Publications website at DOI: 10.1021/acs.nanolett.5b02511.

Details of plane wave density functional theory calculation, InP nanopillar fabrication, energy band diagram of the TiO_2-passivated InP structure and schematic diagram of photoelectrochemical measurement setup are included. Ti 2p level, Cu 2p, and O 1s core level XPS spectra. Faraday efficiencies and time dependence of methanol of 12 h reaction on InP/TiO_2Cu sample illuminated with 532 nm light at an applied overpotential of −0.6 V vs NHE (PDF)

■ AUTHOR INFORMATION

Corresponding Author

*E-mail: scronin@usc.edu.

Author Contributions

J.Q. and G.Z. equally contributed to this paper.

Notes

The authors declare no competing financial interest.

■ ACKNOWLEDGMENTS

This research was supported by ARO Award No. W911NF-14-1-0228 (to J.Q.), NSF Award No. CBET-0846725 (to G.Z.), and Air Force Office of Scientific Research under AFOSR BRI Grant FA9550-12-1-0481 (to A.N.A). This work used the Extreme Science and Engineering Discovery Environment (XSEDE),[33] which is supported by National Science Foundation grant number ACI-1053575.

■ REFERENCES

(1) Halmann, M. *Nature* **1978**, *275*, 115−116.
(2) Inoue, T.; Fujishima, A.; Konishi, S.; Honda, K. *Nature* **1979**, *277*, 637−638.
(3) Canfield, D.; Frese, K., Jr *J. Electrochem. Soc.* **1983**, *130*, 1772−1773.
(4) Aurian-Blajeni, B.; Halmann, M.; Manassen, J. *Sol. Energy Mater.* **1983**, *8*, 425−440.
(5) Barton, E. E.; Rampulla, D. M.; Bocarsly, A. B. *J. Am. Chem. Soc.* **2008**, *130*, 6342−6344.
(6) Shockley, W.; Queisser, H. J. *J. Appl. Phys.* **1961**, *32*, 510−519.
(7) Hoffman, C.; Jarasiunas, K.; Gerritsen, H.; Nurmikko, A. *Appl. Phys. Lett.* **1978**, *33*, 536−539.
(8) Lee, M. H.; Takei, K.; Zhang, J.; Kapadia, R.; Zheng, M.; Chen, Y. Z.; Nah, J.; Matthews, T. S.; Chueh, Y. L.; Ager, J. W. *Angew. Chem.* **2012**, *124*, 10918−10922.
(9) Qiu, J.; Zeng, G.; Pavaskar, P.; Li, Z.; Cronin, S. B. *Phys. Chem. Chem. Phys.* **2014**, *16*, 3115−3121.
(10) Zeng, G.; Qiu, J.; Li, Z.; Pavaskar, P.; Cronin, S. B. *ACS Catal.* **2014**, *4*, 3512−3516.
(11) Hu, S.; Shaner, M. R.; Beardslee, J. A.; Lichterman, M.; Brunschwig, B. S.; Lewis, N. S. *Science* **2014**, *344*, 1005−1009.
(12) Chen, Y. W.; Prange, J. D.; Dühnen, S.; Park, Y.; Gunji, M.; Chidsey, C. E.; McIntyre, P. C. *Nat. Mater.* **2011**, *10*, 539−544.
(13) Morgan, B. J.; Watson, G. W. *J. Phys. Chem. C* **2010**, *114*, 2321−2328.
(14) Lindan, P.; Harrison, N.; Gillan, M.; White, J. *Phys. Rev. B: Condens. Matter Mater. Phys.* **1997**, *55*, 15919.
(15) Krüger, P.; Bourgeois, S.; Domenichini, B.; Magnan, H.; Chandesris, D.; Le Fevre, P.; Flank, A.; Jupille, J.; Floreano, L.; Cossaro, A. *Phys. Rev. Lett.* **2008**, *100*, 055501.
(16) Von Oertzen, G.; Gerson, A. *Int. J. Quantum Chem.* **2006**, *106*, 2054−2064.
(17) Giannozzi, P.; Baroni, S.; Bonini, N.; Calandra, M.; Car, R.; Cavazzoni, C.; Ceresoli, D.; Chiarotti, G. L.; Cococcioni, M.; Dabo, I. *J. Phys.: Condens. Matter* **2009**, *21*, 395502.
(18) Kohn, W.; Sham, L. J. *Phys. Rev.* **1965**, *140*, A1133.
(19) Lee, C.; Yang, W.; Parr, R. G. *Phys. Rev. B: Condens. Matter Mater. Phys.* **1988**, *37*, 785.
(20) Burke, K.; Werschnik, J.; Gross, E. *J. Chem. Phys.* **2005**, *123*, 062206.
(21) Perdew, J. P.; Burke, K.; Ernzerhof, M. *Phys. Rev. Lett.* **1996**, *77*, 3865.
(22) Cococcioni, M.; De Gironcoli, S. *Phys. Rev. B: Condens. Matter Mater. Phys.* **2005**, *71*, 035105.
(23) Finazzi, E.; Di Valentin, C.; Pacchioni, G.; Selloni, A. *J. Chem. Phys.* **2008**, *129*, 154113−154113.
(24) Cheng, H.; Selloni, A. *Phys. Rev. B: Condens. Matter Mater. Phys.* **2009**, *79*, 092101.
(25) Tang, W.; Sanville, E.; Henkelman, G. *J. Phys.: Condens. Matter* **2009**, *21*, 084204.
(26) Sanville, E.; Kenny, S. D.; Smith, R.; Henkelman, G. *J. Comput. Chem.* **2007**, *28*, 899−908.
(27) Henkelman, G.; Arnaldsson, A.; Jónsson, H. *Comput. Mater. Sci.* **2006**, *36*, 354−360.
(28) Kuhl, K. P.; Cave, E. R.; Abram, D. N.; Jaramillo, T. F. *Energy Environ. Sci.* **2012**, *5*, 7050−7059.
(29) Li, Y.; Wang, W.-N.; Zhan, Z.; Woo, M.-H.; Wu, C.-Y.; Biswas, P. *Appl. Catal., B* **2010**, *100*, 386−392.
(30) Gattrell, M.; Gupta, N.; Co, A. *J. Electroanal. Chem.* **2006**, *594*, 1−19.
(31) Chinchen, G. C.; Spencer, M. S.; Waugh, K. C.; Whan, D. A. *J. Chem. Soc., Faraday Trans. 1* **1987**, *83*, 2193−2212.
(32) Hori, Y.; Murata, A.; Takahashi, R. *J. Chem. Soc., Faraday Trans. 1* **1989**, *85*, 2309−2326.
(33) Towns, J.; Cockerill, T.; Dahan, M.; Foster, I.; Gaither, K.; Grimshaw, A.; Hazlewood, V.; Lathrop, S.; Lifka, D.; Peterson, G. D. *Comput. Sci. Eng.* **2014**, *16*, 62−74.
(34) Sorescu, D. C.; Al-Saidi, W. A.; Jordan, K. D. *J. Chem. Phys.* **2011**, *135*, 124701.1−124701.17.

■ NOTE ADDED AFTER ASAP PUBLICATION

This paper was published ASAP on August 14, 2015. A reference (ref 34) has been added, with corresponding revisions to the text (abstract, page C, and concluding paragraph), Figure 3, and the Supporting Information file. The corrected version was reposted on August 19, 2015.

Downloaded by UNIV OF CALIFORNIA LOS ANGELES on September 1, 2015 | http://pubs.acs.org
Publication Date (Web): August 14, 2015 | doi: 10.1021/acs.nanolett.5b02511

DOI: 10.1021/acs.nanolett.5b02511
Nano Lett. XXXX, XXX, XXX−XXX